Proc. of the X Int. Conf. — Ion Implantation and other Applications of Ions and Electrons, Kazimierz Dolny 2014

Investigation of NbN and Nb–Si–N Coatings Deposited by Magnetron Sputtering

V.I. Ivashchenko[a], P.L. Scrynskyy[a], O.S. Lytvyn[b], V.M. Rogoz[c,*], O.V. Sobol[d], A.P. Kuzmenko[e], H. Komsta[f] and C. Karvat[g]

[a]Institute for Problems of Material Science, NASU, Krzhyzhanovsky Str. 3, 03680 Kiev - 142, Ukraine
[b]Institute of Semiconductor Physics, NASU, Nauky Pr. 41, 03028 Kyiv, Ukraine
[c]Sumy State University, Rimsky-Korsakov Str. 2, 40000, Sumy, Ukraine
[d]National Technical University "Kharkiv Polytechnic Institute", Frunze Str. 21, 61002, Kharkov, Ukraine
[e]Kursk State Technical University, Center for collective use "High Tech", 305040, October 50 Str. 94, Kursk, Russia
[f]Institute of Transport, Combustion Engines and Ecology, Lublin University of Technology, Nadbystrzycka 36, 20-618 Lublin, Poland
[g]Department of Electrical Devices and High Voltage Technology, Lublin University of Technology, Nadbystrzycka 36, 20-618 Lublin, Poland

NbN and Nb–Si–N films were deposited by magnetron sputtering the Nb and Si targets on silicon wafers at various bias voltages, U_s. The deposited films were annealed to establish their thermal stability. The films were investigated by atomic force microscope, X-ray diffraction, X-ray photoelectron spectroscopy and nanoindentation. The NbN films were nanostructured, and the Nb–Si–N films had a nanocomposite structure, and represented an aggregation of δ-NbN_x nanocrystallites embedded into the amorphous Si_3N_4 tissue (nc-δ-NbN_x/a-Si_3N_4).

DOI: 10.12693/APhysPolA.128.949

PACS: 61.05.C–, 61.05.cp, 68.37.Ps, 61.05.js

1. Introduction

Nanostructured films are widely used for surface hardening of cutting tools due to high hardness, good corrosion stability, and low friction coefficient [1–7]. Among these films, NbN-based ones are of increasing interest. Hardness of such binary NbN nitride films is much higher than the bulk material ($HV = 14$ GPa) and higher than other binary nitride films (TiN, ZrN, VN). The hardness of the NbN films deposited by different arc deposition systems reaches 34–49 GPa [8]. The NbN films were also prepared by using magnetron sputtering (MS) [9], ion beam assisted deposition [10], pulsed laser deposition [11]. An increase in hardness was reached by the formation of nanocomposite or nanolayered structures of the films based on niobium nitride. Silicon nitrides are known for their high temperature stability, low friction coefficient and high oxidation resistance. Hence, one can expect that Nb–Si–N nanocomposite and multilayers will combine the properties of the constituent materials and will have improved properties as compared to NbN. Furthermore, we will take into account the films prepared using magnetron sputtering. We reviewed the recent investigations on the NbN and Nb–Si–N films deposited by magnetron sputtering.

As follows from this brief review, despite the previous investigations of the NbN and Nb–Si–N films, the comparative study of these two kinds of films prepared with the same deposition parameters has not been carried out yet. Also, so far the effect of the bias voltage supplied to the substrate (U_s) on film properties has not been analyzed.

The aim of this paper was to fill these gaps in the investigations of NbN and Nb–Si–N films. These films were deposited on silicon wafers at various U_s. The films were then investigated by: atomic force microscope (AFM), X-ray diffraction (XRD), X-ray photoelectron spectroscopy (XPS), nanoindentation, and microindentation. The deposited nanocomposite films were annealed to establish their thermal stability.

2. Experimental details

The NbN-based films were deposited on the mirror-polished Si (100) wafer by dc magnetron sputtering the Nb (99.9%, Ø72×4 mm) and Si (99.999%, Ø72×4 mm) targets in an argon-nitrogen atmosphere under the following deposition parameters: substrate temperature $T_s = 350^0$ °C; substrate bias $U_s = 0$ V, –20 V, –40 V, –70 V; flow rates $F_{Ar} = 40$ sccm; $F_{N_2} = 13$ sccm; working pressure $p_C = 0.17$ Pa. The current applied to the Nb target was 150, 200, 250 and 300 mA, which corresponded to a discharge power density P_{Nb} from 8.5 W/cm^2 to 17.1 W/cm^2. The current on the Si target was 100 mA ($P_{Si} =$ 5.3 W/cm^2). The base pressure of the vacuum chamber

*corresponding author; e-mail: v.rogoz2009@gmail.com

was lower than 10^{-4} Pa. The distance between the targets and the substrate holder was 8 cm. The dihedral angle between the target planes was $\sim 45°$. The substrates were cleaned ultrasonically before they were put into the vacuum chamber. Also before deposition, the substrates were etched in the vacuum chamber in hydrogen plasma during 5 min. The film deposited at $P_{\mathrm{Nb}} = 14.3$ W/cm^2 was annealed in a vacuum (0.001 Pa) for 2 hours at 600, 800 and 1000 °C.

The crystal structure of the films was determined by XRD (diffractometer DRON-3M) using the CuK_α radiation. The crystallite size in films was evaluated from the broadening of peaks in the X-ray diffraction spectra using the Scherrer formula. The chemical bonding status of films was observed by XPS (EC 2401 spectrometer, USSR) using the MgK_α radiation (E =1253.6 eV). The Au $4f_{7/2}$ and Cu $2p_{3/2}$ peaks with binding energies at 84.0±0.05 eV and 932.66±0.05 eV, respectively, were used as a reference. Surface morphology was analyzed by atomic force microscope (AFM) NanoScope IIIa Dimension 3000 (Digital Instruments, USA). The hardness and elastic modulus of films were determined from the indentation by a Nanoindenter-G200 instrument equipped with a Berkovich pyramidal tip under load in a range of 9-13 mN. This range of loads was chosen in order to obtain prominent plastic deformation of film while avoiding the influence of substrate material. The nanohardness (H) and elastic modulus (E) data was obtained from load-displacement curves using the Oliver and Pharr method. The Knoop hardness (HK) was estimated by a Microhardness Tester Micromet 2103 BUEHLER Ltd at a loading of 100 mN.

3. Results and discussion

Figure 1 shows the AFM surface topography of the NbN and Nb–Si–N films deposited at various U_s. One can see that the film surface roughness increases with U_s. Also the surface roughness in the Nb–Si–N films is smaller than in the NbN ones, which can be due to the availability of the amorphous SiN_x tissue in the Nb–Si–N films (see below). It follows that a decrease in the bias voltage U_s and introduction of silicon promote the reduction of surface roughness.

The XRD spectra of the deposited NbN and Nb–Si–N films are shown in Figs. 2 and 3. The peak A at 35.1–35.40 and the peak B at 41.1–41.40 can be assigned to the δ-NbN_x(111) and δ-NbN_x(200) reflections, respectively. The grain size estimated from the Scherrer formula was 4.1–8.7 nm and 18.1–19.8 nm for the NbN and Nb–Si–N films, respectively. It follows that introduction of Si leads to an increase of NbN grains.

The results of XPS examination of the as-deposited and annealed NbN and Nb–Si–N films are presented in Fig. 4. It is known that a native oxide grows on Nb compounds when exposed to air [12], and the peaks at 204.07 eV and 206.88 eV can be assigned to Nb 3d in NbN (203.97 eV [13]) and $\mathrm{Nb_2N_{2-x}O_{3+x}}$ (207.0 eV [14]), respectively. For the NbN films, the peak at 397.4 eV in the N 1s spectrum is determined by the Nb-N bonds, whereas for the Nb–Si–N films, this peak is located around 397.2 eV, and can be assigned to N 1s in NbN (397.4 eV [12]).

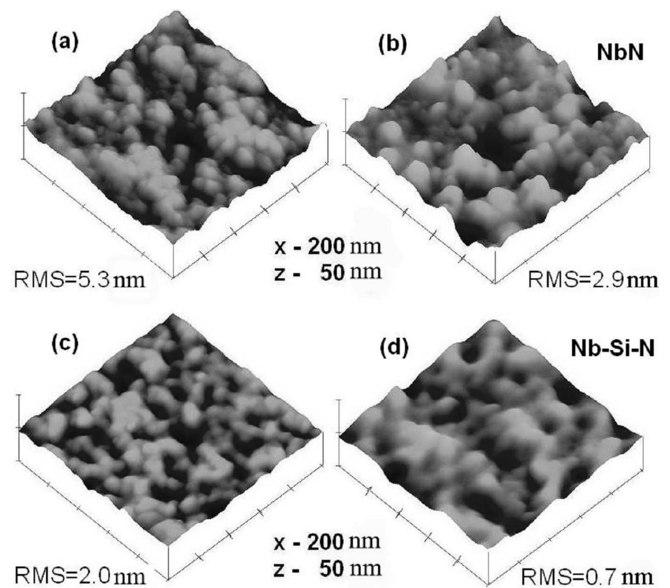

Fig. 1. AFM images of: the NbN films deposited at U_s = 0 V (RMS =5.3 nm) (a) and U_s = −70 V (RMS = 2.9 nm) (b); Nb–Si–N films deposited at U_s = 0 V (RMS = 2.0 nm) (c) and U_s = −70 V (RMS = 0.7 nm) (d).

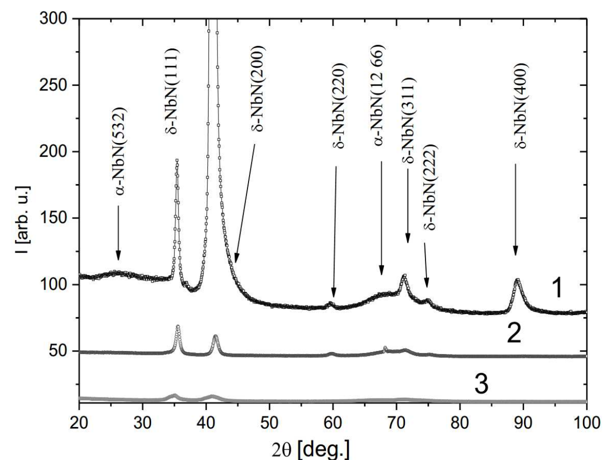

Fig. 2. XRD spectra of NbN films at U_s = 0 V (1), U_s = −40 V (2), U_s = −70 V (3).

We suppose that the asymmetry of the N 1s peak can be caused by the Si-N bonds in $\mathrm{Si_3N_4}$ (397.8 eV [14]). The XPS measurements of the Si 2p spectrum provide further information on the Si bonding in the Nb–Si–N films (cf. Fig. 4). The peak at a binding energy of 101.7 eV is assigned to Si in $\mathrm{Si_3N_4}$ (101.7 eV [14]), and a shoulder at 103.3 eV in the Si 2p spectrum of the annealed films is supposed to be due to the Si-O bonds in $\mathrm{SiO_2}$ (103.5 eV [14]). Finally, the O 1s spectra of the NbN

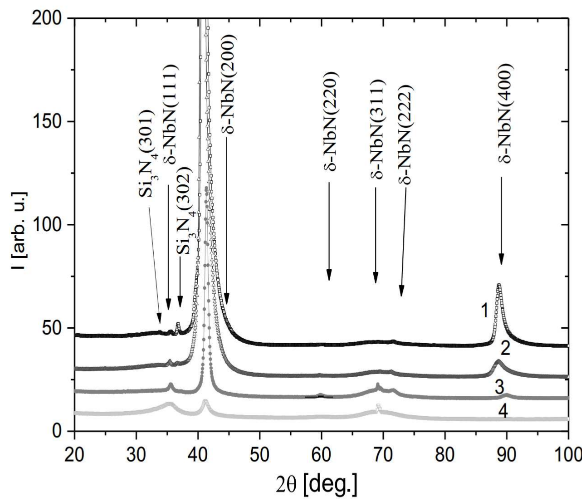

Fig. 3. XRD spectra of Nb–Si–N films at $U_s = 0$ V (1), $U_s = -20$ V (2), $U_s = -40$ V (3), $U_s = -70$ V (4).

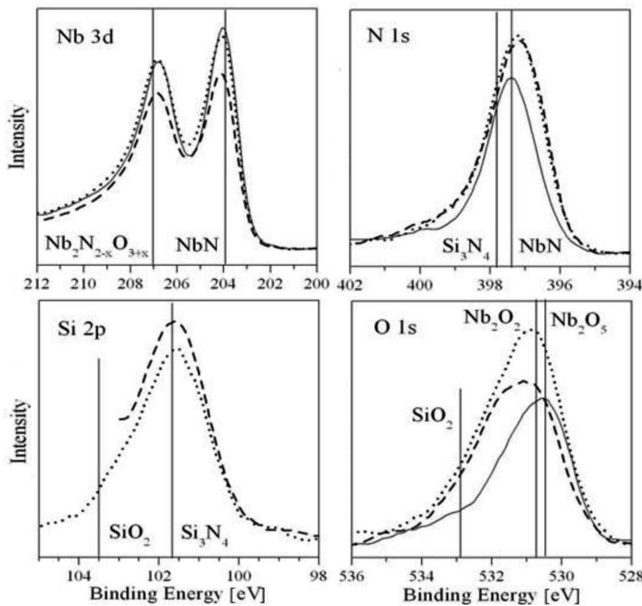

Fig. 4. XPS spectra of the core levels in NbN (solid line), Nb–Si–N (dashed line) and annealed at 1000 °C Nb–Si–N (dotted line) films deposited at P_w = 14.3 W/cm^2. Vertical lines denote the binding energies of the XPS peaks of: Nb 3*d* in NbN, 203.97 eV [13] and $Nb_2N_{2-x}O_{3+x}$, 207.0 eV [14]; N 1*s* in NbN, 397.4 eV [12] and Si_3N_4, 397.8 eV [14]; Si 2*p* in Si_3N_4, 101.7 eV and SiO_2, 103.5 eV [14]; O 1*s* in Nb_2O_5, 530.4 eV, Nb_2O_2, 530.7 eV and SiO_2, 532.9 eV [14].

and Nb–Si–N films are centered around 530.5 eV and 530.9 eV, respectively, and can be attributed to the Nb-O bonds in Nb_2O_5 (530.4 eV) and Nb_2O_2 (530.7 eV [14]), respectively. In the case of Nb–Si–N films, the Si-O bonds in SiO_2 can form the wide tail around 532.9 eV [14] (cf. Fig. 4). Using the XPS data (cf. Fig. 4), we estimated the niobium, nitrogen and silicon contents ($C_{\rm Nb}, C_{\rm N}$ and $C_{\rm Si}$, respectively) in the NbN and Nb–Si–N films. It was found that $C_{\rm Nb}$ = 44.5 at.%, $C_{\rm N}$ = 55.5 at.% for the NbN films and $C_{\rm Nb}$ = 45.1 at.%, $C_{\rm N}$ = 43.2 at.% and $C_{\rm Si}$ = 11.7 at.% for Nb–Si–N films.

Comparison of the results presented in Figs. 1–4 makes it possible to establish the structure of the NbN and Nb–Si–N films. The NbN films are nanostructured, and the Nb–Si–N films have a nanocomposite structure, and represent an aggregation of δ-NbN_x nanocrystallites embedded into the amorphous Si_3N_4 tissue (nc-δ-NbNx/a-Si_3N_4). In contrast to the NbN films, the Nb–Si–N ones are textured with the preferable (200) grain orientation. The films contain oxygen in the view of niobium oxides. For the Nb–Si–N films, we also suppose that oxygen forms SiO_2 that is segregated along grain boundaries. We note that, despite larger grain sizes, the surface roughness of the Nb–Si–N films is smaller as compared to that of the NbN films. One can assume that the amorphous SiN_4 tissue in the nanocomposite Nb–Si–N films smears the relief of the film surface, for this reason, the surface roughness of the nanocomposite films should be lower than that of the NbN films.

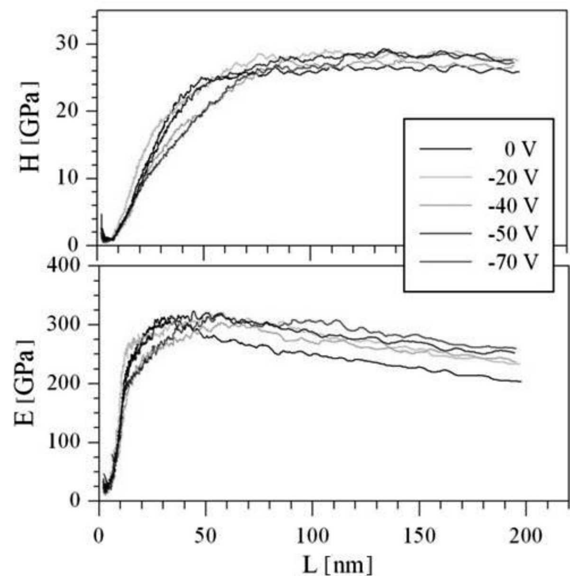

Fig. 5. Dependences of nanohardness (H) and elastic modulus (E) on nanoindenter penetration (L) for the NbN films deposited at various bias voltages.

The dependence of nanohardness (H) and elastic modulus (E) on indenter penetration (L) of the deposited films are presented in Figs 5 and 6. It can be seen that beginning with 75 nm, the nanohardness practically does not depend on L. The elastic modulus decreases upon a reaching maximum values at L = 50 nm. These results point out that the soft silicon substrate does not exert influence on the films nanohardness. The elastic modulus of the films turns out to be more sensitive to the substrates, especially at high L.

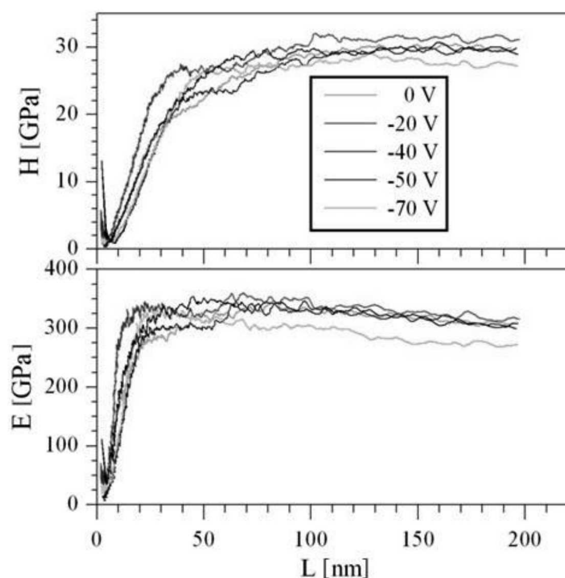

Fig. 6. As Fig. 5 for the Nb–Si–N.

4. Conclusions

We have deposited the NbN and Nb–Si–N films on the silicon wafers by magnetron sputtering at various bias voltages applied to the substrate. The comparative investigation of the deposited films was carried out. The AFM investigations show that decrease in the bias voltage and introduction of silicon promote reduction of surface roughness of the films. The XRD and XPS examinations enabled one to establish the possible structure of the deposited films: the NbN films were nanostructured, and the Nb–Si–N ones had a nanocomposite structure, and represented an aggregation of δ-NbN_x nanocrystallites embedded into the amorphous SiN_x tissue (nc-δ-NbN_x/a-Si_3N_4). In contrast to the NbN films, the Nb–Si–N ones are textured with the preferable (200) grain orientation. The Nb–Si–N films exhibit higher hardness ($H \approx 30$ GPa, $HK \approx 44$ GPa) than the NbN films ($H \approx 28$ GPa, $HK \approx 36$ GPa) mainly due to the formation of the nanocomposite nc-δ-NbN_x/a-Si_3N_4 structure. The elastic modulus of the NbN and Nb–Si–N films increases with the increasing grain sizes.

References

[1] A.D. Pogrebnjak, A.G. Ponomarev, A.P. Shpak, *Phys. Usp.* **55**, 270 (2012).

[2] A.D. Pogrebnjak, V.M. Beresnev, *Nanocoatings, Nanosystems, Nanotechnologies*, Bentham Sci. Pub., Sharjah 2012.

[3] A.D. Pogrebnjak, V. M. Beresnev, A. A. Demianenko, *Phys. Solid State.* **54**, 1882 (2012).

[4] R. Krause-Rehberg, A.D. Pogrebnyak, O.V. Sobol', *Phys. of Metals and Metallogr.* **114**, 672 (2013).

[5] A.D. Pogrebnjak, Yu.A. Kravchenko, S.B. Kislitsyn, *Surface and Coatings Technology* **201**, 2621 (2006).

[6] A.D. Pogrebnjak, S. Bratushka, V.I. Boyko, *Nucl. Instr. Meth.* **145**, 373 (1998).

[7] A.D. Pogrebnjak, A.D. Mikhaliov, A.D., N.A. Pogrebnjak, *Phys. Let.* **241**, 357 (1998).

[8] V.N. Zhytomirsky, *Surf. Coat. Technol.* **201**, 6122 (2007).

[9] G.A. Fontalvo, V. Terziyska, C. Mitterer, *Surf. Coat. Technol.* **202**, 1017 (2007).

[10] N. Hayashi, I.H. Murzin, I. Sakamoto, M. Ohkubo *Thin Solid Films* **259**, 146 (1995).

[11] G. Cappuccio, U. Gambardella, A. Morone, S. Orlando, G.P. Patisi, *Appl. Surf. Sci.* **109**, 399 (1997).

[12] J. Wang, Z. Song, K. Xu, *Surf. Coat. Technol.* **201**, 4931 (2007).

[13] J.J. Jeong, C.M. Lee, *Appl. Surf. Sci.* **214**, 11 (2003).

[14] G. Beamson, D. Briggs, *High Resolution XPS of Organic Polymers, The Scienta ESCA300 Database*, Wiley Interscience 1992.